Acta Crystallographica Section D
Biological Crystallography
ISSN 1399-0047

PLP undergoes conformational changes during the course of an enzymatic reaction

Ho-Phuong-Thuy Ngo,[a,b]‡ Nuno M. F. S. A. Cerqueira,[b]‡ Jin-Kwang Kim,[a] Myoung-Ki Hong,[a,b] Pedro Alexandrino Fernandes,[c] Maria João Ramos[c]* and Lin-Woo Kang[a,b]*

[a]Department of Biological Sciences, Konkuk University, 1 Hwayang dong, Gwangjin-gu, Seoul 143-701, Republic of Korea, [b]Center for Cellular and Structural Biology, School of Pharmaceutical Sciences, Sun Yat-Sen University, Guangzhou, People's Republic of China, and [c]Requimte/Departamento de Química e Bioquímica, Faculdade de Ciências, Universidade do Porto, Rua do Campo Alegre s/n, 4169-007 Porto, Portugal

‡ These authors contributed equally to this paper.

Correspondence e-mail: mjramos@fc.up.pt, lkang@konkuk.ac.kr

Received 2 August 2013
Accepted 14 November 2013

PDB references: XometC, native, 4ixz; EAS and EAA, 4iy7; PGD, EAA and IAI, 4iyo

Numerous enzymes, such as the pyridoxal 5′-phosphate (PLP)-dependent enzymes, require cofactors for their activities. Using X-ray crystallography, structural snapshots of the L-serine dehydratase catalytic reaction of a bacterial PLP-dependent enzyme were determined. In the structures, the dihedral angle between the pyridine ring and the Schiff-base linkage of PLP varied from 18° to 52°. It is proposed that the organic cofactor PLP directly catalyzes reactions by active conformational changes, and the novel catalytic mechanism involving the PLP cofactor was confirmed by high-level quantum-mechanical calculations. The conformational change was essential for nucleophilic attack of the substrate on PLP, for concerted proton transfer from the substrate to the protein and for directing carbanion formation of the substrate. Over the whole catalytic cycle, the organic cofactor catalyzes a series of reactions, like the enzyme. The conformational change of the PLP cofactor in catalysis serves as a starting point for identifying the previously unknown catalytic roles of organic cofactors.

1. Introduction

Pyridoxal 5′-phosphate (PLP), the active form of vitamin B_6, is one of the most versatile organic cofactors (Percudani & Peracchi, 2003; Toney, 2011). PLP-dependent enzymes catalyze more than 140 different enzyme activities, which correspond to over 4% of all classified activities, and include transamination, racemization, decarboxylation and side-chain elimination and replacement in amino-acid metabolism (Clausen *et al.*, 1996). Additionally, these enzymes are also widespread in cellular processes, such as the biosynthesis of amino acids and amino-acid-derived metabolites and in the biosynthetic pathways of amino sugars and other amine-containing compounds.

The crystalline form of vitamin B_6 was first isolated in 1938 (Keresztesy & Stevens, 1938). Since then, the sophisticated mechanisms of PLP-dependent enzyme catalysis have been intensively studied. The currently accepted catalytic mechanism of PLP-dependent enzymes involves complicated electron and proton movements through the extensively conjugated π-bonds of the PLP pyridine ring with various reaction intermediates. Multiple transaldimination reactions are required for each catalytic cycle, in which the PLP cofactor establishes different imine linkages either with the active-site Lys residue or with the substrate and the reaction intermediates (Oliveira *et al.*, 2011; Cerqueira *et al.*, 2011). In addition, conformational change of the PLP cofactor during

catalysis was also observed from experimental data on protein structure, fluorescence and UV–Vis spectral changes, which implied that the PLP cofactor is active in catalysis (Burkhard *et al.*, 1999; Chen & Phillips, 1993; Hayashi *et al.*, 1998, 2003; McClure & Cook, 1994). The specific chemistry that is catalyzed by each enzyme is then dependent on a specific cluster of active-site residues.

PLP-dependent enzymes continue to be a subject of intense investigation, further triggered by the outcome of functional genomics, the improvement in cloning, expression and purification techniques, and the discovery of their involvement in several human diseases, thus calling for specific inhibitors/drugs (Amadasi *et al.*, 2007). Indeed, several PLP-dependent enzymes are already promising targets for the treatment of epilepsy (Mumford & Cannon, 1994), the development of antibacterial and antiviral agents (Milligan *et al.*, 2007; Müller *et al.*, 2009), the treatment of cancer (Snell & Riches, 1989) and to attack parasites such as *Trypanosoma brucei*, the causative agent of African sleeping sickness (Wang, 1995). In addition, functional defects in PLP-dependent enzymes have been implicated in a number of disease pathologies, including homocystinuria (Kraus *et al.*, 1999; Rao *et al.*, 2008).

Despite the long history of research in the field, we are only now beginning to answer some of the most exciting questions. Although many different crystal structures of PLP-dependent enzymes have been determined, they typically only contain the enzyme alone or in complex with a substrate or inhibitor. These structures are insufficient for understanding how the full catalytic process occurs. In this sense, several pieces of experimental evidence require further research.

The *XometC* gene from *Xanthomonas oryzae* pv. *oryzae* was annotated as a cystathionine γ-lyase (CGL)-like protein and classified as an aspartate aminotransferase (AAT)-like fold type I (Grishin *et al.*, 1995). In this study, we identified L-serine dehydratase activity of XometC, which is found in PLP-dependent enzymes that are involved in β-elimination reactions. Crystal structures of XometC were determined from three different crystals consisting of a tetramer in the asymmetric unit, which included an apoenzyme structure from a native crystal and four structures corresponding to different intermediates in the L-serine dehydratase activity from two serine-soaked crystals. Each intermediate structure had a different PLP conformation, which played a different role in each catalytic reaction. These results are complemented by theoretical and computational results that provide atomistic detail regarding the role of PLP during catalysis.

2. Materials and methods

2.1. Crystallization and structure determination

The *XometC* gene (*Xoo0778*) was cloned from *Xanthomonas oryzae* pv. *oryzae* KACC 10331 and the protein was expressed, purified and initially crystallized (Ngo *et al.*, 2008). Crystals appeared at 20°C in a solution consisting of 25.5%(*w*/*v*) PEG 4000, 0.085 *M* Tris pH 9.0, 0.17 *M* $LiSO_4$, 15%(*v*/*v*) glycerol and grew to final dimensions of 0.3 × 0.2 × 0.08 mm within a week. For X-ray diffraction analysis, a crystal was flash-cooled in liquid nitrogen. X-ray data were collected from the cooled crystal (in a nitrogen stream at 100 K) on beamline 4A at the Pohang Light Source (PLS), Republic of Korea. The data set was integrated and scaled using *DENZO* and *SCALEPACK*, respectively (Otwinowski & Minor, 1997). The phases of XometC were obtained by molecular replacement (MR) with *Phaser* in the *CCP*4 software package (McCoy *et al.*, 2007) using human CGL (PDB entry 2nmp; 54% sequence identity; Sun *et al.*, 2009) as a search template. All model building and electron-density interpretations were performed using *Coot* (Emsley *et al.*, 2010). Structures were refined using the *CCP*4 program *REFMAC*5 (Murshudov *et al.*, 2011).

Table 1
Data-collection and refinement statistics.

Values in parentheses are for the highest resolution shell. Each data set was collected from a single crystal.

Crystal	Native (PDB entry 4ixz)	EAS, EAA (PDB entry 4iy7)	PGD, EAA, IAI (PDB entry 4iyo)
Soaking time with serine		10 min	11 h
Data collection			
Space group	$P2_12_12_1$	$P2_12_12_1$	$P2_12_12_1$
Unit-cell parameters			
a (Å)	78.8	76.5	76.3
b (Å)	86.3	86.1	86.3
c (Å)	223.4	226.0	226.3
$\alpha = \beta = \gamma$ (°)	90.0	90.0	90.0
Resolution (Å)	50.0–2.07 (2.11–2.07)	50.0–1.67 (1.70–1.67)	50.0–1.78 (1.81–1.78)
R_{merge} (%)	9.1 (38.0)	9.2 (55.1)	11.1 (62.0)
$\langle I/\sigma(I)\rangle$	43.4 (8.7)	30.5 (3.2)	24.1 (2.9)
Completeness (%)	99.7 (99.3)	99.2 (85.5)	99.7 (95.3)
Multiplicity	14.5 (13.5)	8.8 (7.5)	9.8 (8.1)
Refinement			
Resolution (Å)	40.25–2.07	30.23–1.70	33.82–1.80
No. of reflections	88708	155517	132060
R_{work}/R_{free} (%)	18.0/24.6	13.4/16.9	13.6/18.0
No. of atoms			
Protein	11485	11584	11585
Ligand/ion			
Bicarbonate	4	ND	ND
Serine	ND	28	35
Iminopropionate	ND	ND	12
Aminoacrylate-PLP	ND	21	21
Serine-PLP	ND	66	ND
Pyruvate	ND	12	6
Water	918	1424	1324
B factors (Å^2)			
Protein	22.8	13.8	16.7
Ligand/ion			
Bicarbonate	24.0	ND	ND
Serine	ND	20.1	26.2
Iminopropionate	ND	ND	30.3
Aminoacrylate-PLP	ND	13.5	18.6
Serine-PLP	ND	16.3	ND
Pyruvate	ND	28.1	26.3
Water	30.3	26.8	26.4
R.m.s. deviations			
Bond lengths (Å)	0.024	0.030	0.028
Bond angles (°)	1.972	2.262	2.128
Ramachandran statistics (%)			
Allowed	9.4	8.5	7.3
Most favoured	90.3	91.1	91.6
Outliers	0.3	0.5	0.5

To obtain reaction-intermediate structures, crystals were transferred into crystallization solution supplemented with 10 m*M* L-serine for various durations. More than 50 diffraction data sets were collected from a number of different soaked crystals on beamline 17A of the Photon Factory (KEK) in Japan. The determined XometC structure was used as a search template to solve the complex structures by MR and rigid-body refinement in *CCP*4. The catalytic intermediate structures were determined from two different crystals soaked for 10 min and 11 h. All structures were validated using *WHAT IF* (Vriend, 1990) and *SFCHECK* (Vaguine *et al.*, 1999). The final data-collection and refinement statistics are shown in Table 1. Graphical representations were created using *PyMOL* (v.1.3r1; Schrödinger). A PLP-linked Lys molecule (IT1) with a double-bonded Schiff-base linkage from the *Coot* monomer library was used for the native structure (Vagin *et al.*, 2004). All other library files of ligands were prepared using the *Mono Library Sketcher* from the *CCP*4 package (Winn *et al.*, 2011).

2.2. Computational methodology

To evaluate the reactions involved in the conversion of the internal aldimine to the external aldimine, a simplified model system for theoretical calculations was built that contained a simplified version of the PLP cofactor in which both the phosphate and the methyl groups were replaced by H atoms. The active-site lysine and the amino substrate were replaced by methylamines, so that the formation and cleavage of the *gem*-diamine intermediate would be the same reversible reaction and the free energy could be studied in a single step. All studies were performed using *Gaussian* 09 (Frisch *et al.*, 2009) and density functional theory was used. The geometry

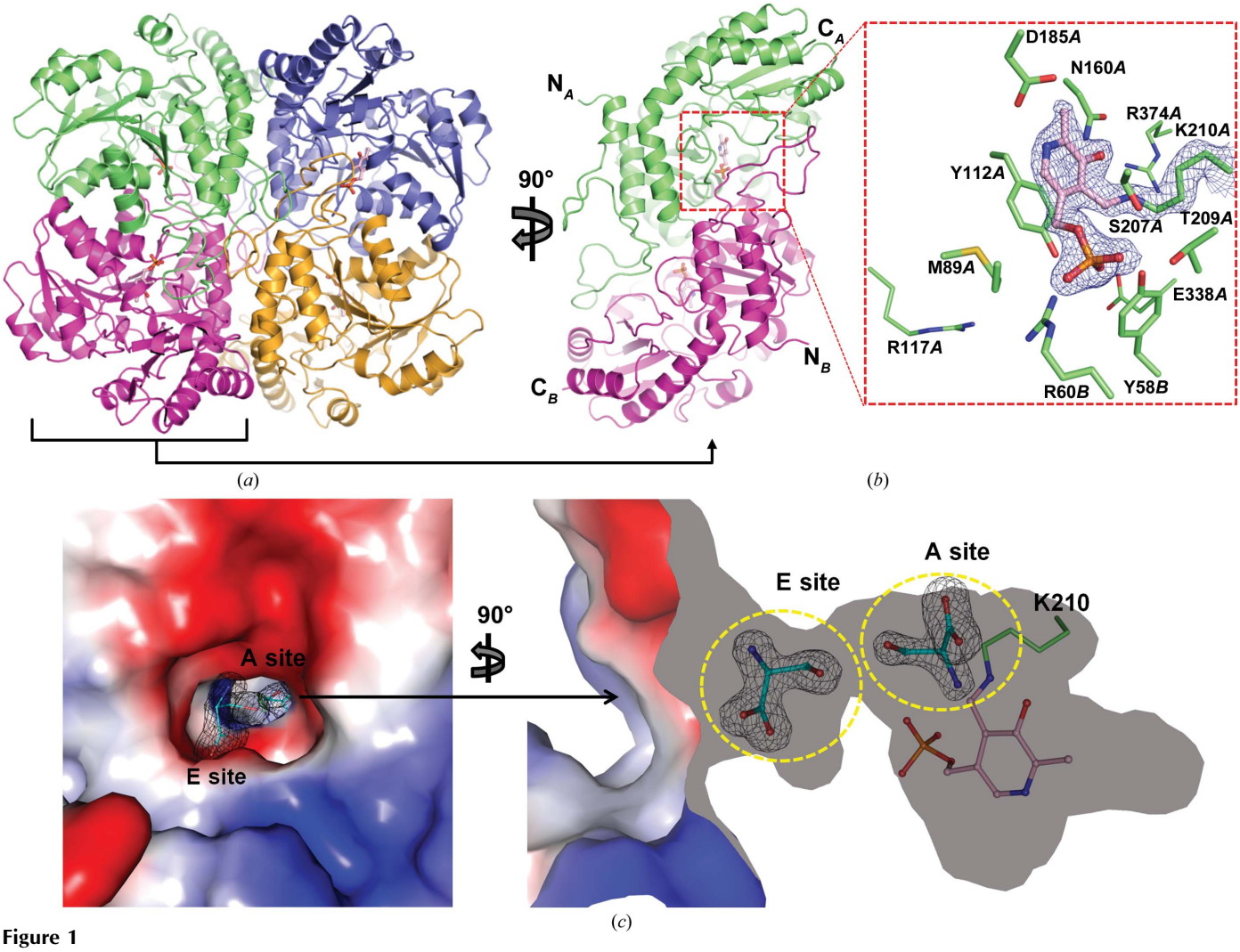

Figure 1
Crystal structure of XometC. (*a*) Homotetramer structure of XometC with two dimers related by a twofold rotation axis. One dimer is shown in light magenta and lime and the other in bright orange and slate. Each protomer contains one PLP cofactor. The PLP cofactors are shown as a light pink ball-and-stick representation. (*b*) Dimer of XometC rotated 90° compared with (*a*). The colours are the same as in (*a*). The red dashed square shows the active site with the PLP. The blue contours at 1.0σ represent the $2F_o - F_c$ map of the internal Schiff base in the native structure. N_A and N_B and C_A and C_B are the N- and C-termini of protomers *A* and *B*, respectively. The last letter (*A* or *B*) of the residue labels indicates the chain ID. (*c*) Electrostatic surface representation showing two serine-binding sites (E and A sites) in the active-site channel. Left, direct view from the outside to the inside of the channel. Right, black-face culling of the surface to generate the inside view of the active-site channel; the view is rotated to the left by 90° relative to the figure on the left. The E and A sites are marked by yellow dashed circles. Serine residues are shown as a cyan ball-and-stick representation.

optimizations were performed using the M06 functional (Zhao & Truhlar, 2008*a*,*b*) and the 6-31+G(d) basis set for all atoms. In all of the calculations, the following protocol was used. We first searched for the transition state starting from the reactants, using a scan in which the reaction coordinate of interest was shortened or stretched. The transition states were subsequently fully geometrically optimized (except for the dihedral angle, which was fixed at the angle of interest) starting from the structure at the highest energy point of the scans. The associated reactants and products were determined by internal reaction coordinate (IRC) calculations. In all cases, the stationary points were obtained using standard Gaussian convergence criteria. The transition-state structures were identified by vibrational frequency calculations, as there was exactly one imaginary frequency with the correct transition vector, even when using frozen atoms, which shows that the frozen atoms were almost free from steric strain. Zero-point corrections and thermal and entropic effects (T = 310.15 K, P = 100 kPa) were added to all of the calculated energies with the 6-311++G (3d,2p) basis set. In order to evaluate the effect of the dihedral angle in the conversion of the internal/external aldimine and the *gem*-diamine intermediate, geometric optimizations of the model system were conducted at fixed values of the dihedral angle of the Schiff-base linkage, but the same protocol as described before was followed.

3. Results

3.1. Crystal structure of XometC

All previously characterized CGLs and cystathionine β-lyases (CBLs) were tetramers (Clausen *et al.*, 1996; Sun *et al.*, 2009; Messerschmidt *et al.*, 2003), and the purified XometC protein, a CGL-like protein with 54% sequence identity to human CGL, also existed as a tetramer in nondenaturing gel

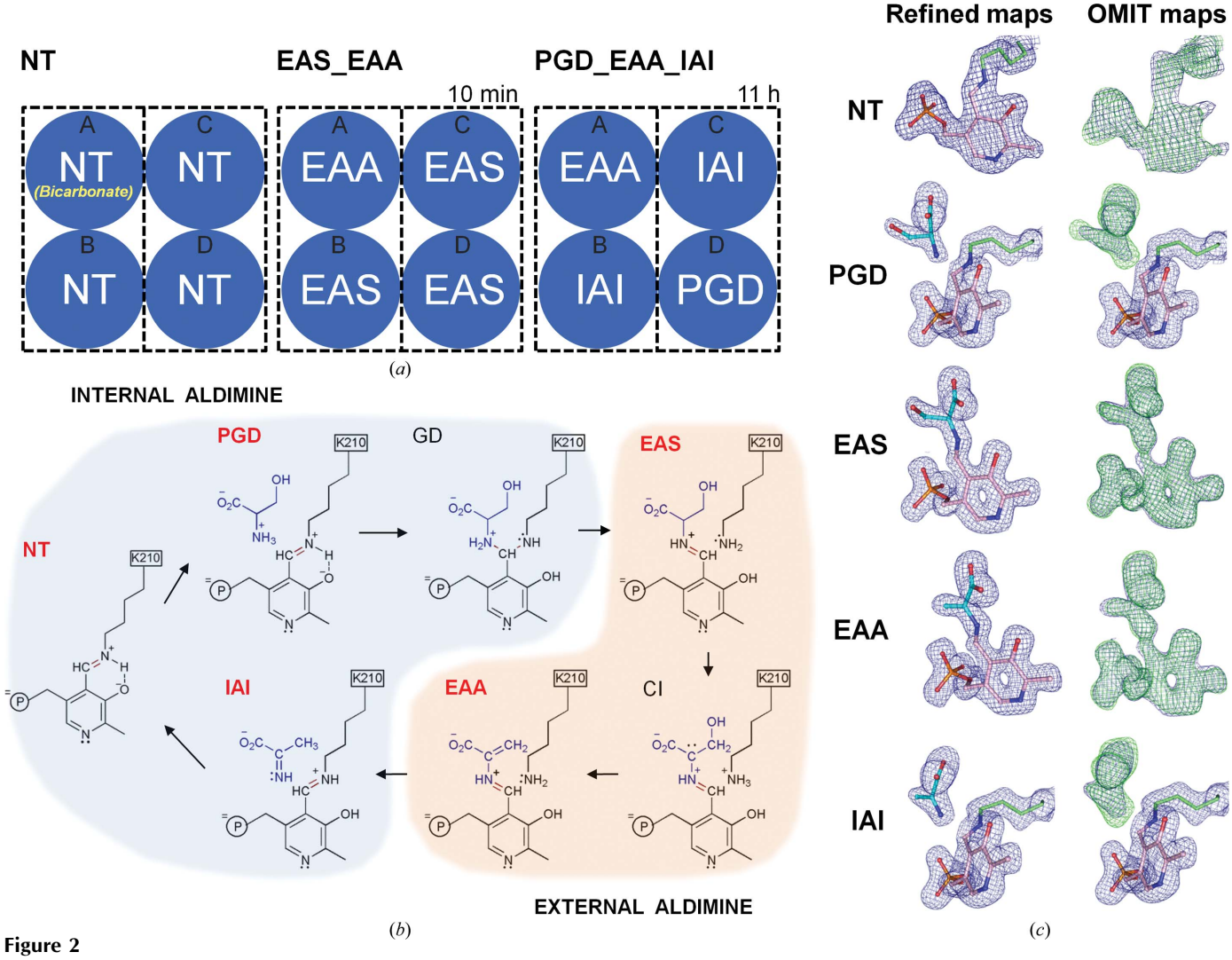

Figure 2
Tetramers in XometC crystals and intermediate crystal structures. (*a*) Four protomers of the tetramer in the asymmetric unit of XometC crystals. Dashed boxes represent active dimers in the tetramer. (*b*) Catalytic reaction scheme of XometC for serine substrate. The five catalytic steps determined by X-ray crystallography are indicated in bold red letters. (*c*) Apoenzyme structure and four intermediate structures of XometC and their refined and OMIT maps. Blue, $2F_o - F_c$ map (contoured at 1.0σ); green, $F_o - F_c$ map (contoured at 3.0σ). The OMIT maps were generated without the PLP-linked Lys (in the NT structure), without serine/iminopropionate ligands (in the PGD/IAI structures) and without serine external Schiff-base/aminoacrylate external Schiff-base ligands (in the EAS/EAA structures).

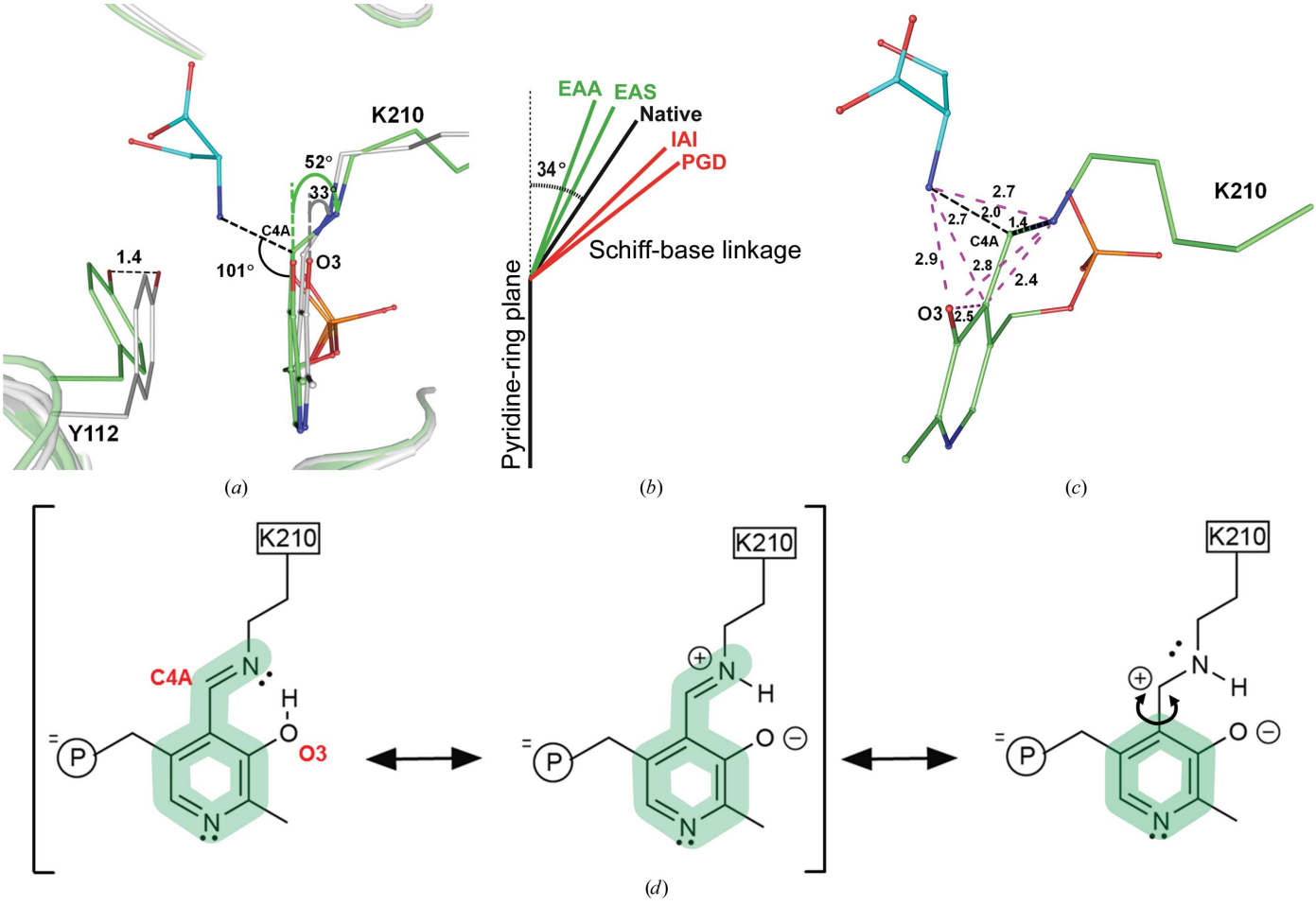

Figure 3
PLP dihedral angles in crystallographic intermediate structures. (*a*) Superimposition of the active sites of the NT structure (chain *D*) and the PGD structure. The tilted dihedral angle of the native XometC structure (silver) is further twisted by an additional 19° in the PGD structure (green). (*b*) Comparison of the average dihedral angles in intermediate structures. Internal aldimine structures in the transaldimination reaction (PGD and IAI) showed higher dihedral angles than external aldimine structures (EAS and EAA) that have extensive π-bond conjugation. (*c*) Tetrahedral geometry of PLP and attacking and leaving amino groups in PGD. (*d*) Schematic representations of chemical structures of Schiff-base-linked PLP: resonance structures of Schiff-base-linked PLP. Structures in parentheses show the double-bond forms of the Schiff-base linkage, in which the O3 atom can have the enol form (left) or the keto form (middle). The right structure shows the single-bond form of the Schiff-base linkage with the keto form of the O3 atom.

electrophoresis. XometC crystals were obtained at pH 9.0, and the native XometC structure was determined by MR at 2.07 Å resolution using human CGL (PDB entry 2nmp; Sun *et al.*, 2009) as a search model (Table 1). There were four protomers in the asymmetric unit, with two active dimers related by twofold noncrystallographic symmetry forming a tetramer (Figs. 1*a* and 1*b*). Each protomer interacted with its neighbours through more than 10% of its surface area: protomer *A* had contact areas of 2451 Å^2 (16%) out of 15 542 Å^2 with protomer *B* and 1486 Å^2 (10%) with protomer *C*. The protomer structure could be divided into three regions: an N-terminal domain (residues 14–64) consisting of an α-helix and an extended loop, which interacted with the active site of the adjacent protomer; a large PLP-binding domain (residues 65–260) consisting of seven mainly parallel β-strands covered by seven α-helices and two 3_{10}-helices, which included most of the catalytically important residues; and a C-terminal domain (residues 261–392) consisting of five α-helices, one 3_{10}-helix and four antiparallel β-strands.

Each active site was made of residues from both protomer *A* and protomer *B* of an active dimer, and each active site contained a PLP molecule. The protomer conformation was affected by ligand binding, and the four protomers of the XometC tetramer behaved independently in this respect. For example, in the native XometC structure protomer *A* was in a closed conformation with a bicarbonate ion in the active site and the other three protomers were in open conformations with no ligands in the active sites. In the bicarbonate-bound protomer *A*, the C-terminal domain was shifted closer to the PLP-binding domain by a maximal 2.7 Å displacement of the helix–loop–helix motif (residues 351–361), which did not interact directly with the substrate but played an important role in building the substrate-binding pocket (Supplementary Fig. S1[1]).

[1] Supporting information has been deposited in the IUCr electronic archive (Reference: DW5070).

The PLP cofactor was clearly seen near the C-termini of the β_4, β_5 and β_6 strands and the N-terminus of the α_3 helix. The PLP was covalently joined to the ε-amino group of the active-site Lys210 through a Schiff-base linkage (Steegborn & Clausen, 2000), resulting in the signature absorption peak (λ_{max}) at 423 nm (Karsten & Cook, 2002; Supplementary Fig. S2*a*) and the yellow colour of the XometC crystals. The PLP made many additional interactions with both protomers of the active dimer (Fig. 1*b*): the phosphate group of the PLP was hydrogen-bonded to the main chains of Gly88 and Met89 of protomer *A* and the side chain of Arg60 of protomer *B*; the pyridoxal ring of the PLP was within van der Waals distance of The87 and Ser207 on one side and Tyr112 on the opposite side and was stacked on the phenol ring of Tyr112 of protomer *A*; and the N atom of the pyridoxal ring was stabilized by a hydrogen bond to Asp185.

3.2. Intermediate structures and their dihedral angles

We also determined the intermediate structures of the L-serine dehydratase activity (β-elimination activity towards L-serine) of XometC. PLP-dependent enzymes frequently show catalytic promiscuity, such that one enzyme exhibits more than one catalytic activity (Percudani & Peracchi, 2003). We confirmed the catalytic activity of XometC by enzyme assays using spectroscopy (Supplementary Table S1) and HPLC (Supplementary Fig. S2*b*). The results confirmed both γ-elimination and β-elimination activities of XometC. All of the substrates/substrate analogues were used to attempt to obtain co-crystal structures. Hundreds of crystals were soaked with the putative substrates L-cystathionine, L-*O*-succinylhomoserine, L-homoserine, L-homocysteine, L-cysteine and

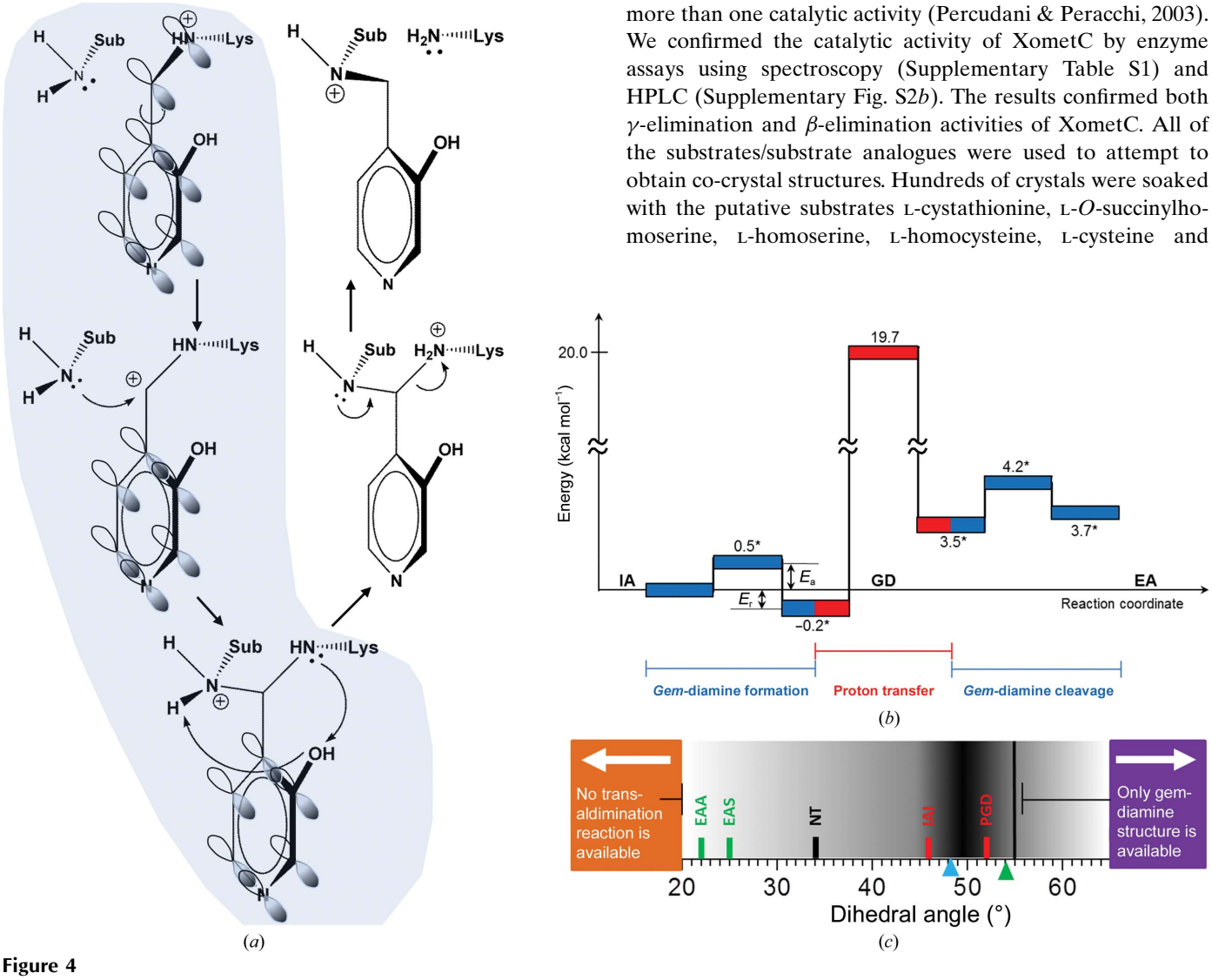

Figure 4
The simplified model for high-level quantum-mechanical calculations and free-energy calculations of each intermediate state from the internal aldimine (IA) to the external aldimine (EA). (*a*) The simplified model of the transaldimination reaction for high-level quantum-mechanical calculations. The structures just prior to nucleophilic attack, of the *gem*-diamine and after completion of transaldimination are shown. Free energies for half of the transaldimination reaction (shaded part) were calculated. The π-bond conjugation in the pyridine ring and the Schiff-base linkage in the shaded part are indicated by balloons. (*b*) The activation free energy (E_a) and the reaction free energy (E_r) of *gem*-diamine formation and cleavage are indicated in blue, and those of the concerted proton transfer are indicated in red. Values labelled with an asterisk were calculated with a dihedral angle of 48° between the PLP ring and the Schiff-base linkage. (*c*) Rotation of the dihedral angle in different catalytic steps. The average dihedral angles of different catalytic intermediate structures are shown in the same colour as in Fig. 3(*b*). The most preferred dihedral angles for transaldimination are shown as dark shadows between the IAI and PGD structures. All five average angles were within the possible range of calculated dihedral angles for interconversion between the internal/external aldimine and the *gem*-diamine. The range of dihedral angle rotation was limited between approximately 20 and 52° by the active-site geometry of XometC and the conformation of the Lys210 side chain. The cyan triangle shows the best calculated angle of 48° for *gem*-diamine formation and the green triangle shows the best calculated angle of 52° for concerted proton transfer.

L-serine at various concentrations, and we tried to collect diffraction data. However, we were only able to collect diffraction data from serine-soaked crystals.

When we soaked the substrates into the XometC crystals, the colour of the crystals changed depending on the substrate and the soaking time. We attempted to collect X-ray diffraction data from as many as possible of the diverse substrate-soaked crystals. However, for most of the samples we could not collect diffraction data or could only collect data to low resolution owing to smeared diffraction spots and high mosaicity of the crystals. Only with the serine-soaked crystals did we manage to collect two diffraction data sets to higher than 1.8 Å resolution, after soaking times of 10 min and 11 h (Fig. 2*a*).

The serine-soaked XometC structures showed two clear positive electron densities near the PLP: one at the entrance to the hydrophilic channel leading to the active site, which we designate the entry (E) site, and the other adjacent to the PLP, which we refer to as the active (A) site (Fig. 1*c*). Surprisingly, the individual protomers in the two serine-soaked crystals exhibited four different catalytic steps in the L-serine dehydratase activity (Fig. 2). The L-serine dehydratase activity of XometC was also confirmed by an enzyme kinetics assay (Supplementary Fig. S3). The structures included (i) the internal aldimine structure just before *gem*-diamine (GD) formation with the substrate L-serine (pre-*gem*-diamine structure with L-serine; PGD); two external aldimine structures, (ii) a structure resembling a reaction intermediate just after the formation of the external aldimine with the substrate L-serine (external aldimine structure with L-serine; EAS) and (iii) an aminoacrylate structure obtained after the β-elimination reaction (external aldimine structure with aminoacrylate; EAA); and (iv) the internal aldimine structure with iminopropionate, which is the final product of the catalytic process (internal aldimine structure with existing iminopropionate; IAI).

The key finding from the intermediate structures was the conformational change of the PLP dihedral angle between the pyridine ring and the Schiff-base linkage in each intermediate. The PLP dihedral angle varied between 18 and 52° (Fig. 3*b*). Larger dihedral angles (43–52°) were present in the structures just before the transaldimination reaction with a substrate, *i.e.* PGD, and just after the release of a product from the second transaldimination reaction, *i.e.* IAI. The external aldimine structures EAS and EAA had smaller dihedral angles (18–34°), and the native structure NT showed more flexible dihedral angles around 34° (Supplementary Table S2). The ideal geometry between the pyridine ring and the Schiff-base linkage is a co-planar conformation to maximize the extensive π-bond conjugation and generate hydrogen bonds between the O3 atom and the Schiff-base N atom. However, the dihedral angle of the native XometC was twisted by approximately 34°, and in the PGD structure the dihedral angle was further distorted to 52° as the substrate approached the PLP (Fig. 3*a*).

3.3. Tetrahedral structure in PGD

A PGD dihedral angle of 52° generates an almost perfect tetrahedral structural relationship between the PLP O3 atom and both the attacking and leaving amino groups (Fig. 3*c*). In the PGD structure, the O3 atom can play a novel catalytic role in the concerted proton transfer from the substrate to the Lys210 amino group. The O3 atom can exist in either a ketoenamine or an enolimine form (Fig. 3*d*); the negatively charged ketoenamine form (the catalytically active form) can abstract a proton from the substrate amino group. This abstraction will perturb the pre-existing hydrogen bond between the O3 atom and the Schiff-base N atom, which facilitates rotation of the dihedral angle. When the dihedral angle rotates, the PLP Schiff-base linkage also contributes to the nucleophilic attack of the substrate on the C4A atom of

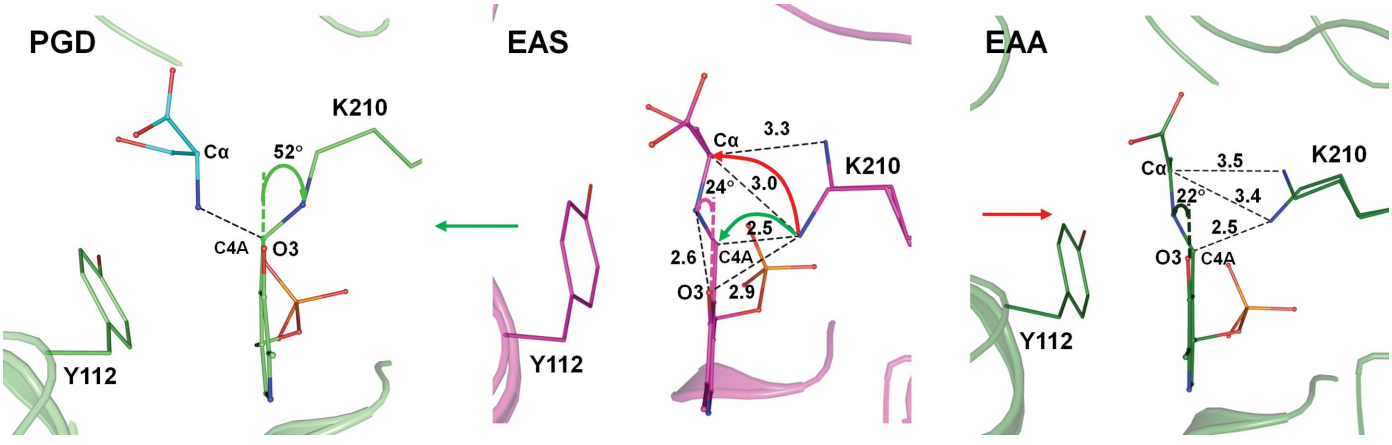

Figure 5
The dihedral angle decides the catalytic path for deprotonation of the C^{α} atom. In EAS, the ε-amino group of Lys210 has dual positions from which to attack the substrate C^{α} atom (red arrow) or the C4A atom (green arrow). The dihedral angle of 24° leads to preferential deprotonation of the substrate C^{α} atom, leading to the EAA structure *via* a β-elimination reaction rather than the reverse transaldimination attack on the C4A atom to return to the NT structure.

the PLP. The PLP Schiff-base linkage adopts one of two resonance forms: a single or a double bond. The single-bond form of the Schiff-base linkage is more flexible for dihedral angle rotation because it is free from π-bond conjugation with the pyridine ring, where the C4A atom is more positively charged, which facilitates nucleophilic attack of the deprotonated amino group of the substrate (Fig. 3*d*).

3.4. Quantum-mechanical calculations for the transaldimination reaction

To evaluate and confirm the influence of the PLP dihedral angle during the catalytic process, high-level computational methods were used (Ramos & Fernandes, 2008; Zhao & Truhlar, 2008*a*). We built a model system capable of representing the intrinsic reactivity of the PLP/Lys/substrate system, as described in the methods §2.2 (Fig. 4*a*). The computational results confirmed that conversion between the internal aldimine and the external aldimine requires three sequential steps. The first is the conversion of the internal aldimine to a *gem*-diamine intermediate. In the second step, a proton is transferred from the substrate to the active-site lysine. This reaction is catalyzed by the enol group of the PLP ring, which acts as a proton shuttle between both amino groups of the substrate and the active-site lysine. The third step is the formation of the external aldimine, which is basically the reverse reaction of the first step. The full energetic profile of these three reactions is very favourable: the complete reaction is almost thermoneutral (3.7 kcal mol^{-1}, where 1 cal = 4.186 J; Fig. 4*b*).

The computational results also revealed that conversion between the internal/external aldimine and the *gem*-diamine intermediates is optimal only when the dihedral angle of the Schiff base linkage is around 48° (Supplementary Fig. S4). Under such conditions, the interconversion of these two states can occur with almost no energetic cost. The rate-limiting step is the coupled proton transfer process, which requires an activation energy of 20.0 kcal mol^{-1}, and the reaction is endothermic by 3.7 kcal mol^{-1}. This reaction occurs best when the dihedral angle of the Schiff-base linkage is around 55°, which is very similar to the dihedral angle that was obtained for the PGD structure (52°). The PGD and IAI structures resemble the reactant or the product of the transaldimination reactions. The computationally determined minimum showed that the *gem*-diamine intermediate generated an almost perfect tetrahedral structure, similar to PGD, with an optimal configuration for the essential concerted proton transfer.

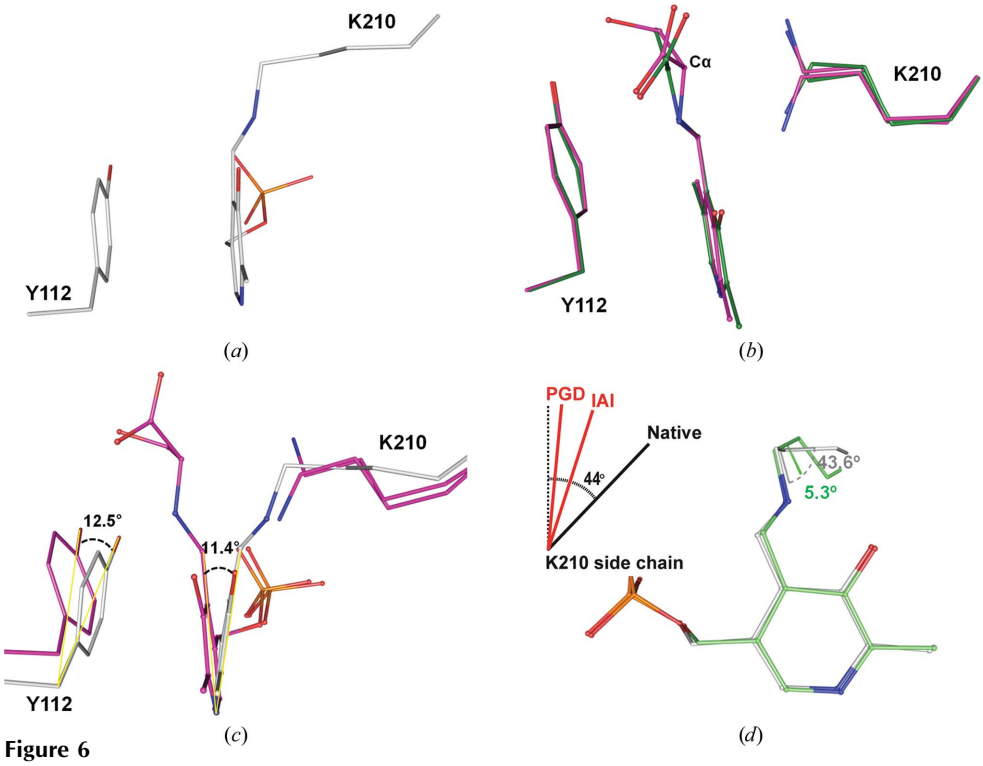

Figure 6
Restraint of dihedral angle rotation by the XometC active-site geometry. (*a*) In the NT structure, the pyridine ring is stacked with Tyr112. (*b*) In the external aldimine structures, both the pyridine ring and the Tyr112 side chain are tilted. Tyr112 makes van der Waals interactions with the substrate serine attached to the PLP rather than the pyridine ring, which holds the dihedral angle at around 20°. (*c*) Superimposed structures of PLP in the NT and EAS structures. (*d*) The conformations of the terminal end of the Lys210 side chain in the NT and PGD structures. In the PGD structure, the terminal four atoms of the Lys210 side chain had a more compressed structure (dihedral angle of 5.3°) compared with the rather relaxed form in NT (dihedral angle of 43.6°). Accordingly, the Lys210 side-chain conformation in PGD prohibits further rotation of the PLP dihedral angle above 52°. The inset figure shows the dihedral angles of the terminal four atoms of the Lys210 side chain in the intermediate structures.

3.5. Carbanion formation *via* specific dihedral angle conformation

After the EAS structure has formed, the dihedral angle changes to approximately 25°, at which the freely released ε-amino group of Lys210 can deprotonate the substrate C$^{\alpha}$ atom to form the carbanion intermediate (forward direction) or re-attack the PLP C4A atom to return to the NT structure (reverse direction; Fig. 5). Although the interatomic distances are suitable for both reactions, the EAS dihedral angle of 25° makes transaldimination energetically unfavourable (Fig. 4*c*) and promotes the forward reaction of carbanion formation.

Theoretical results proposed that an equilibrium between the internal/external aldimine and *gem*-diamine intermediates only exists when the dihedral angle of the Schiff base is in the range 22–65° (Fig. 4*c*). Below 22° only the internal or the external aldimine exists, whereas above 65° only the *gem*-diamine intermediate is

found. The active-site structure restrained the PLP dihedral angle within the available range of the transaldimination reaction. In the EAS and EAA structures, Tyr112 limits the dihedral angle to around 20° (Fig. 6). In the PGD structure, the terminal end of the Lys210 side chain has a dihedral angle of about 5°, which is more strained than the 44° of Lys210 in the NT structure (Fig. 6*d*). The stressed conformation of Lys210, like a compressed coil, may prohibit further rotation of the dihedral angle beyond 52°. Accordingly, the reaction intermediate will not remain in the GD structure. These overall results show that the PLP dihedral angle is a molecular switch for the catalytic reaction.

3.6. Full catalytic cycle of the L-serine dehydratase activity with dihedral angle conformational change

Here, we propose the catalytic mechanism of the L-serine dehydratase activity in terms of PLP conformational changes; this provides the simplest mechanism to explain the catalytic process, with a net zero movement of protons or electrons from outside for the whole cycle (Supplementary Video S1). The proposed steps of the transaldimination mechanism and carbanion-intermediate formation are conserved and are applicable to most PLP-dependent enzymes.

In the native state (NT), the PLP is covalently bound to Lys210 through a Schiff-base linkage and the pyridoxal ring is stacked on the phenol ring of Tyr112. The dihedral angle between the pyridine ring and the Schiff-base linkage is 34°. When the substrate serine enters at the E site of the substrate-binding pocket, the phenyl ring of Tyr112 is tilted towards the E site by 1.4 Å, resulting in a loss of the π-stacking interaction with the pyridoxal ring of the PLP. The serine moves to the open A site and its amino group is deprotonated by the O3 atom of the PLP pyridoxal ring. The dihedral angle between the pyridine ring and the Schiff-base linkage is further distorted to 52°. At the increased dihedral angle, the extended π-bond system between the Schiff base and the pyridine ring is disrupted. As a result, the Schiff-base linkage has more single-bond character than double-bond character. Simultaneously, the C4A atom attains a more positively charged character. Accordingly, the deprotonated nucleophilic amino group attacks the C4A atom of the PLP, and the resulting pyridoxal ring is tilted 11.4° towards the serine, enabling covalent-bond formation with the serine amino group and restoring the interactions with Tyr112. However, the van der Waals interactions of Tyr112 are greater with the Schiff-base linkage and the covalently attached serine rather than the pyridine ring of the PLP. The side chain of Lys210 is released and can adopt two different conformations, both of which are close enough to deprotonate the C^{α} atom of the serine attached to the PLP. Upon this deprotonation, a carbanionic reaction intermediate is formed, which may be stabilized by delocalization of the nonbonded electrons to the Schiff base and the pyridine ring through a quinonoid structure. Ultimately, transfer of the nonbonded electrons towards the C^{β} atom leads to the β-elimination reaction. The leaving OH^{-} group can acquire a proton from the nearby positively charged protonated N atom of the Schiff base. The β-elimination reaction results in the aminoacrylate-PLP (EAA) structure. The protonated ε-amino group of Lys210 is then deprotonated by the O3 atom of the PLP pyridoxal ring to perform nucleophilic attack on the C4A atom of PLP; the mechanism is similar to the just described transaldimination reaction, but in the reverse direction (from external aldimine to internal aldimine). In the resulting IAI structure, an iminopropionate molecule is released and Lys210 restores a covalent bond to PLP. After the iminopropionate molecule moves out of the binding pocket, Tyr112 returns to its initial position where it is stacked on the pyridoxal ring of PLP. In solution, the iminopropionate molecule would be spontaneously hydrolyzed to a pyruvate molecule by water. We also found electron density for a putative pyruvate molecule on the surface of XometC.

4. Discussion

In the XometC tetramer, each protomer seems to perform the catalytic reaction independently or individually (Fig. 2*a*). If the catalytic status of the first protomer affects the catalytic properties of the remaining three protomers, the observed catalytic steps in the crystals should be organized. This was not the case for XometC. In addition, the initial velocity of XometC at various concentrations of L-serine followed Michaelis–Menten kinetics and there was no allostericity or cooperativity (Supplementary Fig. S3).

With four independent protomers, it was interesting how each XometC protomer in the tetramer became trapped in different catalytic steps coherently in the near-infinite crystal lattice. When we compared all of the XometC protomer structures by superposition, the overall structures of the ligand-bound protomers were very similar, except for the conformation of PLP and nearby residues in the active site (Supplementary Table S3). A structural difference only existed between the liganded and the unliganded protomer structures. The unliganded protomer structures in the native crystal showed a root-mean-square deviation (r.m.s.d.) of approximately 0.3 Å from the liganded protomers. We could not find structural differences between the protomers in different catalytic steps disturbing the XometC crystal lattice. In the native XometC crystal, protomer *A* has a bicarbonate molecule in the active site and its overall conformation was the closed conformation as observed for the other ligand-bound protomers in the serine-soaked crystals. Several CBL structures have also beeen reported to have a bicarbonate molecule in their active sites (Breitinger *et al.*, 2001; Clausen *et al.*, 1996).

There was another hint to the properties of the different intermediate structures. In the electron densities of the EAS and EAA OMIT maps, the imine C atom of the PLP was much weaker than the rest of the molecule (Fig. 2*c*). Because the *B* factors of the PLP and the bound ligands were reasonably low, this weak density was not owing to low occupancies of the ligands (Table 1). We think that the weak density map results, at least partially, from conformational averaging of the PLP between multiple states, which is possible if we consider the

very similar structures of all of the liganded protomers. Accordingly, we should keep in mind that although the observed PLP dihedral angle represented a single catalytic step, it could be an average with other partially mixed steps. The rotation range of the PLP dihedral angles could be wider than that observed in the crystal structures owing to the structural averaging effects.

The L-serine dehydratase activity of XometC is much lower than its lyase activity for cystathione (CTT); the catalytic efficiency (k_{cat}/K_m) of XometC for L-serine is less than 1% of that for the canonical substrate CTT (Supplementary Table S1). The L-serine molecule is very similar to half of the pseudo-symmetric CTT (Supplementary Fig. S5). L-Serine at the E site was held tightly by 12 hydrogen bonds, which prohibited the reaction product from being released from the A site and slowed the catalytic reaction. The inhibition and slow kinetics for L-serine significantly contribute to the capture of the various crystallographic snapshots.

Despite its slower activity towards L-serine, XometC retained its activity and performed the consecutive catalytic reactions in the crystal. We determined the structures of four different catalytic states from two crystals soaked with serine for 10 min and 11 h (Fig. 2*a*). In the 11 h soaked crystal, the PGD structure was observed, which is an earlier catalytic step than the EAS and EAA structures observed in the 10 min soaked crystal. Thus, we believe that the soaking duration is irrelevant in capturing the different intermediate structures.

The intermediate crystal structures showed that the PLP molecule directs the sequence of catalytic reactions by modulating its dihedral angle according to the requirements of the reaction. The PLP molecule (i) deprotonates the substrate amino group using the O3 atom, (ii) attracts nucleophilic attack on PLP itself using the deprotonated amino group of the substrate by switching the Schiff-base linkage state from a double to a single bond, (iii) performs the concerted proton transfer between the substrate amino groups to Lys210 *via* a tetrahedral structure and (iv) directs the reaction to carbanion intermediate formation by allowing deprotonation of the C^{α} atom by Lys210, rather than the backward nucleophilic attack on PLP to return to the native internal aldimine structure. All of the catalytic reactions were controlled by PLP conformations, especially the change in the dihedral angle from 34° to 52° to 22° and again to 34°. Protein enzymes take care of most cellular functions by catalyzing diverse and sophisticated biochemical reactions. Our study provides a new insight in that the PLP prosthetic group itself performs protein-like catalytic reactions with active conformational changes in the protein scaffold.

In the catalytic mechanisms of most PLP-dependent enzymes, the transaldimination reaction and carbanion formation are essential and are well conserved. Many PLP-dependent enzymes such as γ-aminobutyric acid aminotransferase (GABA-AT), L-3,4-dihydroxyphenylalanine (DOPA) decarboxylase, ornithine decarboxylase, methionine γ-lyase and alanine racemase are important drug targets for neurological diseases, cancers and epidemic pathogenic bacteria. Their substrate analogues are already in medical use as first-line drugs (Amadasi *et al.*, 2007; Wu *et al.*, 2011). The detailed catalytic mechanism of the PLP cofactor constitutes important knowledge for the purposes of drug development.

We thank Dr Roger Kornberg for critical discussions, Dr Sang-Hee Lee for reading the manuscript and Dr Hee-Wan Kang for the *XometC* gene. We are also grateful to staff members for their assistance with beamline 4A at the Pohang Light Source (PLS), Republic of Korea and with beamline 17A at the Photon Factory, Japan. This work was supported by grants from the Next-Generation BioGreen 21 Program (No. PJ009500), the Rural Development Administration, Republic of Korea, by the Marine and Extreme Genome Research Center Program of the Ministry of Land, Transportation and Maritime Affairs, Republic of Korea and by the Introduced Innovative R&D Team Leadership of Guangdong Province, People's Republic of China. This work was also supported by FCT through project EXCL/QEQ-COM/0394/2012 and grant No. PEst-C/EQB/LA0006/2011. The authors declare no conflicts of interest.

References

Amadasi, A., Bertoldi, M., Contestabile, R., Bettati, S., Cellini, B., di Salvo, M. L., Borri-Voltattorni, C., Bossa, F. & Mozzarelli, A. (2007). *Curr. Med. Chem.* **14**, 1291–1324.
Breitinger, U., Clausen, T., Ehlert, S., Huber, R., Laber, B., Schmidt, F., Pohl, E. & Messerschmidt, A. (2001). *Plant Physiol.* **126**, 631–642.
Bruinenberg, P. G., De Roo, G. & Limsowtin, G. (1997). *Appl. Environ. Microbiol.* **63**, 561–566.
Burkhard, P., Tai, C.-H., Ristroph, C. M., Cook, P. F. & Jansonius, J. N. (1999). *J. Mol. Biol.* **291**, 941–953.
Cerqueira, N. M. F. S. A., Fernandes, P. A. & Ramos, M. J. (2011). *J. Chem. Theory Comput.* **7**, 1356–1368.
Chen, H. & Phillips, R. S. (1993). *Biochemistry*, **32**, 11591–11599.
Clausen, T., Huber, R., Laber, B., Pohlenz, H. D. & Messerschmidt, A. (1996). *J. Mol. Biol.* **262**, 202–224.
Emsley, P., Lohkamp, B., Scott, W. G. & Cowtan, K. (2010). *Acta Cryst.* D**66**, 486–501.
Esaki, N. & Soda, K. (1987). *Methods Enzymol.* **143**, 459–465.
Frisch, M. J. *et al.* (2009). *Gaussian* 09. Gaussian Inc., Wallingford, Connecticut, USA.
Grishin, N. V., Phillips, M. A. & Goldsmith, E. J. (1995). *Protein Sci.* **4**, 1291–1304.
Hayashi, H., Mizuguchi, H. & Kagamiyama, H. (1998). *Biochemistry*, **37**, 15076–15085.
Hayashi, H., Mizuguchi, H., Miyahara, I., Nakajima, Y., Hirotsu, K. & Kagamiyama, H. (2003). *J. Biol. Chem.* **278**, 9481–9488.
Karsten, W. E. & Cook, P. F. (2002). *Methods Enzymol.* **354**, 223–237.
Keresztesy, J. C. & Stevens, J. R. (1938). *J. Am. Chem. Soc.* **60**, 1267–1268.
Kraus, J. P. *et al.* (1999). *Hum. Mutat.* **13**, 362–375.
McClure, G. D. Jr & Cook, P. F. (1994). *Biochemistry*, **33**, 1674–1683.
McCoy, A. J., Grosse-Kunstleve, R. W., Adams, P. D., Winn, M. D., Storoni, L. C. & Read, R. J. (2007). *J. Appl. Cryst.* **40**, 658–674.
Messerschmidt, A., Worbs, M., Steegborn, C., Wahl, M. C., Huber, R., Laber, B. & Clausen, T. (2003). *Biol. Chem.* **384**, 373–386.
Milligan, D. L., Tran, S. L., Strych, U., Cook, G. M. & Krause, K. L. (2007). *J. Bacteriol.* **189**, 8381–8386.
Müller, I. B., Wu, F., Bergmann, B., Knöckel, J., Walter, R. D., Gehring, H. & Wrenger, C. (2009). *PLoS One*, **4**, e4406.
Mumford, J. P. & Cannon, D. J. (1994). *Epilepsia*, **35**, Suppl. 5, S25–S28.

Murshudov, G. N., Skubák, P., Lebedev, A. A., Pannu, N. S., Steiner, R. A., Nicholls, R. A., Winn, M. D., Long, F. & Vagin, A. A. (2011). *Acta Cryst.* D**67**, 355–367.
Ngo, P.-T. H., Kim, J.-K., Kim, H., Jung, J., Ahn, Y.-J., Kim, J.-G., Lee, B.-M., Kang, H.-W. & Kang, L.-W. (2008). *Acta Cryst.* F**64**, 750–753.
Oliveira, E. F., Cerqueira, N. M. F. S. A., Fernandes, P. A. & Ramos, M. J. (2011). *J. Am. Chem. Soc.* **133**, 15496–15505.
Otwinowski, Z. & Minor, W. (1997). *Methods Enzymol.* **276**, 307–326.
Percudani, R. & Peracchi, A. (2003). *EMBO Rep.* **4**, 850–854.
Ramos, M. J. & Fernandes, P. A. (2008). *Acc. Chem. Res.* **41**, 689–698.
Rao, T. N., Radhakrishna, K., Mohana Rao, T. S., Guruprasad, P. & Ahmed, K. (2008). *Indian J. Dermatol. Venereol. Leprol.* **74**, 375–378.
Snell, K. & Riches, D. (1989). *Cancer Lett.* **44**, 217–220.
Steegborn, C. & Clausen, T. (2000). *Rec. Res. Dev. Biochem.* **2**, 191–207.
Sun, Q., Collins, R., Huang, S., Holmberg-Schiavone, L., Anand, G. S., Tan, C.-H., van-den-Berg, S., Deng, L.-W., Moore, P. K., Karlberg, T. & Sivaraman, J. (2009). *J. Biol. Chem.* **284**, 3076–3085.
Toney, M. D. (2011). *Biochim. Biophys. Acta*, **1814**, 1405–1406.
Uren, J. R. (1987). *Methods Enzymol.* **143**, 483–486.
Vagin, A. A., Steiner, R. A., Lebedev, A. A., Potterton, L., McNicholas, S., Long, F. & Murshudov, G. N. (2004). *Acta Cryst.* D**60**, 2184–2195.
Vaguine, A. A., Richelle, J. & Wodak, S. J. (1999). *Acta Cryst.* D**55**, 191–205.
Vriend, G. (1990). *J. Mol. Graph.* **8**, 52–56.
Wang, C. C. (1995). *Annu. Rev. Pharmacol. Toxicol.* **35**, 93–127.
Winn, M. D. *et al.* (2011). *Acta Cryst.* D**67**, 235–242.
Wu, F., Christen, P. & Gehring, H. (2011). *FASEB J.* **25**, 2109–2122.
Zhao, Y. & Truhlar, D. G. (2008*a*). *Acc. Chem. Res.* **41**, 157–167.
Zhao, Y. & Truhlar, D. G. (2008*b*). *Theor. Chem. Acc.* **120**, 215–241.